Journal of the Indian Institute of Science
A Multidisciplinary Reviews Journal
ISSN: 0970-4140 Coden-JIISAD

REVIEWS

Rigorous Design and Optimization of a New Generation of Optical Sensors

B.M. Azizur Rahman, N. Kejalakshmy, Charusluk Viphavakit, Christos Themistos, Muttukrishnan Rajarajan and K.T.V. Grattan*

Abstract | The design and optimization of a suite of novel optical sensors is presented, showing the value of using rigorous full-vectorial numerical approaches. Although fibre based optical sensors are well established in the market, designs based on more exotic nanowires and photonic crystal fibres are becoming increasingly important and showing much improved sensitivity by accessing a larger evanescent field. Similarly, novel planar design concepts, such as the silicon slot guide-based design is showing even greater promise, allowing the exploitation of well developed CMOS fabrication technologies for potentially low-cost sensor elements. Some selected results illustrating the value and potential of the numerically efficient finite element method in systems design are presented.

1 Introduction

Although the emergence of photonics as a subject has initiated major research and development work for high data rate communication systems, the field has broadened and photonics is also identified as a key enabling technology with its applications across many diverse fields. In particular, there is a growing potential for the exploitation of photonics in sensing applications, for the better measurement of various physical, chemical and biological variables, including pressure, strain, temperature, magnetic field, current, rotation, acceleration, displacement, pH, humidity and a range of gas, chemical and environmental sensing. Sensors play a key role in engineering today and the world market for optical sensors has been continuously growing, and is valued in the several billions of dollar range annually.

One of the main advantages of optical sensors stems from the fact that optical waveguides can be purely dielectric, and thus can be used in hazardous conditions where conventional electric sensors are not be safe. Optical sensors are also immune to electromagnetic interference, and are light weight and potentially more reliable than mechanical sensors. So far most of the well-developed optical sensors are fibre optic based, and with the rapid development in manufacturing technology, more compact planar designs are showing their potential for new sensor designs. In this paper, some of these emerging design concepts for sensing applications are considered showing the value of efficient numerical methods in the design process.

2 Sensor Principles

A sensor converts a measurable physical quantity into a signal, often an electronic signal which can readily be manipulated or measured. Sensors can be classified by the nature of the applications or the measurand, e.g. being physical sensors, chemical sensors, or biosensors. They can also classified into intrinsic or extrinsic. For a fibre optic sensors, when the fibre itself is used as the sensing element, an intrinsic sensor is created; however, when fibre is used only to guide light signal remotely from a sensing element to the optical element where the light interacts with the measurand, an extrinsic sensor device is created. This paper looks at the use of numerical modelling techniques to design *both* types of sensor.

In applications in biomedicine and biotechnology, sensors that detect analytes, such as cells, protein, nucleic acid or biomimetic polymers, are termed biosensors—these are becoming increasingly important bio-analytical tools in the pharmaceutical, biotechnology, food control,

City University London, Northampton Square, London EC1V 0HB, UK.
**b.m.a.rahman@city.ac.uk*

environmental monitoring and other consumer-oriented industries. The development of effective and selective biosensors is currently one of the most active areas of research that can be supported by advanced numerical modelling, creating a very attractive approach for many different applications.

Optical sensors can also be classified by the *principle* they exploit as the basis of the sensing mechanism. Fluorescent-based sensors typically exploit the delay time of the fluorescent signal or the ratio of the optical intensity at two or more wavelengths when excited by light at a shorter wavelength. The use of Fibre Bragg Gratings (FBGs), which are perturbed in a reproducible way by the measurand exploits the sensitivity of the reflected optical signal ultimately to the sensing parameter. However, Long Period Gratings (LPG) that show a different and more complex spectral signature, exploit the coupling of core mode to the cladding modes and the sensitivity of that interaction to the sensing medium. In evanescent sensors, the modal field is accessed in the cladding region, and earlier designs used polished fibre to access the evanescent field. However, more recent designs using nanowires exploit sub-wavelength operation to access the higher evanescent field at the waveguide boundary. Again advanced modelling techniques can reduce the time and costs involved in the design of such sensors.

Plasmonic sensors have also been well established using metal-coated side-polished optical fibre. At the interface between two media whose dielectric constants have opposite signs (e.g. metal and dielectrics), there exist charge-density oscillations giving rise to the Surface Plasmon Wave (SPW). When this wave comes in contact with the analytes, the usually TM-polarized SPW undergoes a phase change, and this phase change is measured and can be related as proportional to the quantity of analytes present. Here the phase matching between the core mode and a plasmonic mode which is influenced by the adjacent sensing media is exploited. In this case, when phase matching is achieved, power couples to highly lossyplasmonic modes and the sensitivity to this power loss forms the basis of the sensing principle.

In the early generation of SPR probes, mostly multimode optical fibres were used. Single mode fibre has also been used to fabricate fibre optic SPR probes where the surface plasmon resonance sensor concept using side-polished single mode optical fibre and a thin metal over layer has been exploited widely. In this configuration, the guided mode propagating in the fire excites the surface plasmon wave at the interface between the metal and a sensing medium. A resonance occurs if the two modes are closely phase matched. Therefore, variations in the refractive index at the sensor surface induced by the interaction between the target analyte molecules in the sample and a biomolecular recognition element (e.g. an antibody) immobilized on the sensor surface may be observed in terms of changes in the resonant wavelength. Such a single-mode optical fibre based SPR sensor is more sensitive and more accurate in comparison to those designed with multi-mode optical fibres. However, the fabrication processes involved are much more complex and sophisticated compared with those that use multi-mode fibres. An advantage of a side-polished half block SPR sensor is that it requires a very small amount of sample, such as in an application for measuring the refractive index of a liquid.

An important concept in optical sensing is to exploit changes in phase or intensity due to the presence of the sensing medium. For example, simple Mach-Zehnder based sensors exploit the differential phase in two parallel arms, where one arm can be used as the reference arm. Alternatively, in a ring resonator, the presence of sensing materials influences the phase of a mode for complete transit along the ring perimeter, and this may be used to find resonating wavelength of the drop port.

There are now many methods that allow the direct detection of biological analytes without labels. Label-free detection generally involves a transducer capable of directly measuring some physical property of the chemical compound, DNA molecule, peptide, protein, virus, or cell. For example, as biochemical molecules and cells have finite mass, volume, viscoelasticity, dielectric permittivity and conductivity, these are properties that can be used to indicate the presence or absence of the molecule using an appropriate sensor. The sensor functions as a transducer that can convert one of these physical properties (such as the mass of a substance deposited on the sensor active surface) into a quantifiable signal, which can be monitored by an appropriate instrument (such as a current or voltage proportional to the deposited mass). Label-free detection removes experimental uncertainty induced by the effect of the label on molecular conformation, blocking of active binding epitopes, steric hindrance, inaccessibility of the labelling site, or the inability to find an appropriate label that functions equivalently for all molecules in an experiment. Label-free detection methods greatly simplify the time and effort required for assay development while

removing experimental artefacts from quenching, shelf life and background fluorescence.

Thus, based on the above, fibre based sensors have been well developed and are increasingly being used in many different types of instrumentation. In the 1980s, many research group were developing optical sensors using polished fibres, in so doing often exploiting sensitive plasmonic coupling of the modes. Recently, nanowires were fabricated by heating and drawing slowly to achieve a sub-wavelength dimension, where the evanescent field could easily be accessed, thus showing greater potential in sensor applications. In 1996, a major new development was reported by Russel *et al*., who introduced a new concept of optical waveguides which could be fabricated with a single material. In this case, a Photonic Crystal Fibre (PCF) with many small air-holes running parallel along the waveguide was developed creating a fibre with highly controllable dispersion and mode shape properties. However, for the sensing communities, the presence of air-holes in the fibre makes it highly attractive by allowing access to the strong field in the air-holes near the core, thus being able to control the modal properties of the waveguide by filling these air-holes with materials on which a measurement can be made.

Integrated optical waveguides are generally more compact than conventional optical systems as they use a higher index contrast between the core and cladding, thereby allowing a much smaller bending radius than in the fibres. Thus, the smaller bending radius will allow more components to be placed in a moderate sized chip, and silicon photonics, exploiting well developed CMOS technology. Another novel concept is the optical slot waveguide, where light guided in a low-index region is important, as this allows an unprecedented nature of access to high optical field in the hollow air-region that can be controlled by the sensing materials. The setup costs for PIC based designs are much higher, but in this case sensors can be mass produced and once the capital market is setup, much lower unit costs can be achieved.

Terahertz (THz) technology, exploiting the spectral region which lies between the very well developed microwave and the optical frequency spectral areas, shows enormous potential for fields such as imaging, and has wide potential in sensing applications. The wavelengths correspond to a wide range of resonant frequencies for many biological and chemicals, creating a momentum for the development of a range of new sensors exploiting this frequency band.

3 Numerical Methods

The availability of the best tools for numerical modelling greatly facilitates the design of a wide range of optical systems. For any guided wave device, the first priority is to obtain modal solutions of these waveguides, where the key parameters are likely to be the effective index, the spatial variation of the full-vectorial field profile, the confinement factor, the mode size, dispersion, and modal and leakage loss. For a circularly symmetric low-index contrast optical fibre, a simple scalar approach in the solution of the problem may be adequate. However, for a high-index contrast, such as is seen in silicon nanowires, with nonlinear or anisotropic materials, or with a complex shape (such as is seen for a PCF), a more rigorous full-vectorial approach would be necessary. Most of the commercial modal solvers available today use the finite difference approach, or field expansions; however, some of the few exploiting computationally efficient finite element method (FEM) are becoming increasingly popular. For the modal solutions of the equations describing these systems, the **H**-field based FEM[1] has been established as one of the most suitable method for all practical optical waveguides.

For most optical waveguides, the refractive index is real, unless the modal loss or gain needs to be introduced, and in that case, its refractive index also has a small imaginary term. On the other hand, thin metal layer supporting plasmonic modes have a very large imaginary term for their refractive index, which makes the real part of the permittivity negative. Early fibre optic sensors used plasmonic modes to absorb optical power in metal layers. However, in more recent photonic devices, the exotic modal properties in plasmonic layers are exploited to design nano-plasmonic resonators to create highly novel sensors.

Some optical sensors will have a component that can be approximated as a waveguide with a uniform cross-section, where a modal solution is applicable. However, it may be necessary to change the cross-section of the structure, which may be continuously or abruptly varied, where the Beam Propagation Method (BPM) would be more useful to apply. The first report of the BPM used Fourier transforms[2] and most of the commercial BPM packages are Finite Difference Method (FDM)-based; however, a FEM based BPM[3] approach would be computationally more efficient. For the analysis of a bent guide, although a BPM approach can be used, a simple conformable transformation[4] would be computationally more efficient.

Whenever there is a discontinuity between two guided wave sections, the tangential electric and magnetic fields must be continuous at that interface. This will cause some reflection of the incident wave and the generation of higher order guided and radiated modes to satisfy the necessary boundary conditions. To analyze such a discontinuity, a simple overlap integral method can be used; however, it has been shown that a full vectorial least squares boundary residual method[5] would be more rigorous to find the necessary scattering coefficients at the interface. However, when several such discontinuity interfaces exist, such as in a Bragg grating, then an approach like the Transfer Matrix Method[6] can be used.

Although a BPM approach can be used to find the evolution of the beam along the guided-wave structures, if it is important to consider the reflected waves at the junction interfaces, then a variant of the BPM, known as the Bi-directional BPM or a more general time-domain approach, would be necessary. In this regard, the well-established and versatile Finite Difference Time Domain (FDTD) Method[7] can be considered, but this approach is computationally expensive for a truly 3-dimensional structures.

Besides the study of light propagation through an optical waveguide or guided wave device, sometimes it is also necessary to exploit other physical effects in the design of the sensors. Polarization-maintaining fibres are often used in optical sensors, and in order to study modal properties of highly birefringent fibres such as the so-called Panda fibre,[8] besides using optical models, it is necessary to calculate the spatial variations of the stress profile (which is tensor), and from that, calculation of the refractive index changes (which are anisotropic) due to the elasto-optic nature of the material can be carried out. In a way it is similar to the study of the Stimulated Brillouin Scattering (SBS) effect in an optical fibre, it is necessary to study acoustic wave propagation[9] through such fibres. Similarly, to the study of temperature effects or the use of thermal tuning of sensors or filters, it is necessary to solve the related Poisson's equation to obtain the 3-dimenstional temperature profile of the sensor. So in a modern optical sensor, the refractive index can be linear, nonlinear, isotropic, anisotropic, or complex, and the structure may either be complex shaped or contain a limited number or many periodic discontinuities, such as Bragg gratings, and accordingly there is a need for effective numerical methods or their combinations to enable their usage in more effective modelling of the devices.

4 Illustrations of the Value of Numerical Methods in Systems Design

In this section, numerically simulated results for several types of emerging optical sensors are presented. To begin with, a conventional polished metal clad optical fibre example is shown, followed by the design approach for sub-wavelength nanowires, photonic crystal fibres, and slot-waveguides. In the modal solution approach based on the use of the FEM, the intricate cross section of a waveguide can be represented by using many triangles of different shapes and sizes. This flexibility makes the FEM preferable compared to the use of the Finite Difference Method (FDM), which not only uses inefficient regular spaced meshing but also cannot represent slanted or curved dielectric interfaces accurately. The optical modes in high contrast metal/dielectric waveguides, with two-dimensional confinement, are also hybrid (polarization mixing) in nature, with all the six components of the **E** and **H** fields being present, and consequently a scalar-FEM analysis will not be valid. For this type of structure, since the **E**-field based formulation cannot represent correctly the boundary condition at the dielectric interfaces (without adding a cumbersome surface integral), only a **H**-field based full vectorial formulation can accurately calculate their modal solutions, which is[1] used here to study the modal solutions.

4.1 *Polished optical fibres*

The SPR structure as shown in Fig. 1 is studied here. This kind of structure has become common in many different sensors because it has been observed that its behaviour is strongly dependent on the refractive index of the surrounding medium. Although a side polished fibre design may also be used, in order to study the effect of fibre parameters on optical properties, a circularly symmetric structure is considered here.

A metal-coated mono-mode optical fibre is considered for the better understanding of the various loss mechanisms and, subsequently, the design and optimization of the biosensor for the detection of *E. coli* was studied. The thickness of the gold metallic layer is taken as 21 nm, with

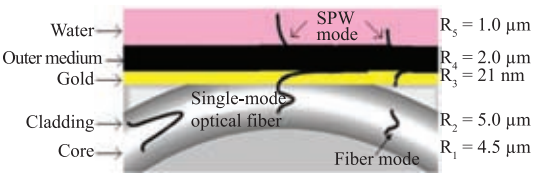

Figure 1: Schematic of the SPR structure studied.

a refractive index of $n = 0.52 + j\,10.7$. The refractive index of the core and cladding are taken as 1.44868 and 1.44439 respectively, at an operating wavelength of 1550 nm. Here, R_1 is the radius of the core and R_2, R_3, R_4, and R_5, are the thicknesses of the cladding, gold, outer medium and water layers respectively.

Initially, R_1, the radius of the core is taken as 4.5 μm, the cladding layer thickness is R_2 is varied from 5–10 μm, the thickness of the gold, R_3 is taken as 21 nm, R_5 as 1.0 μm, and R_4, the outer medium thickness, was varied from 2 μm to 3 μm. The values of the effective indices for the modes of the structures are represented as a function of the outer medium refractive index, R_4. The refractive index of outer medium was varied from 1.440–1.453 to study the coupling between the Inner Surface Plasmon Mode (ISPM) and the Outer Surface Plasmon Mode (OSPM). There are two metal/dielectric interfaces which can support SPM: one at the outer gold/dielectric boundary and the other at the inner gold dielectric boundary. In this waveguide, the mode with the dominant H_x field at the upper and lower metal-dielectric interfaces is tangential to these boundaries, which satisfies the electric-wall boundary condition $\mathbf{n}.\mathbf{H} = 0$ and supports two SPMs along these metal/dielectric interfaces. These two surface plasmon modes have different propagation constants. However, if the propagation constants are closer for these two modes then the two modes can couple and form a supermode or super SPM.

As shown in Fig. 2, as the refractive index of the outer medium increases the effective index difference between the Outer Surface Plasmon Mode (OSPM) and the Inner Surface Plasmon Mode (ISPM) becomes closer and at phase matching condition they are nearly equal. The propagation constants of the two SPMs are close at refractive indices of 1.449, 1.448 for cladding thickness of 5 μm and 10 μm respectively. In this case, the outer medium thickness was fixed at $R_4 = 2$ μm.

Next, the *E. coli* layer with a refractive index value of 1.370 was added to top of the outer medium layer, R_4 with phased matched refractive index values of 1.449 and 1.448 for cladding thickness of 5 μm and 10 μm respectively. The variation of the optical properties with the metal thickness, t, and the outer cladding materials can be better explained with the aid of the field distribution along the radial direction of the fibre and particularly near the dielectric/metal and metal/dielectric interfaces. The variations of the H_x field along the *y*-axis and the *x*-axis for the outer SPM are shown in Fig. 3.

Next the effect of the coupling length with the cladding thickness was studied for cases of with and without *E. coli*. As can be seen from Fig. 4, the coupling length increases monotonically for small values of thickness, and it reaches a maximum around the optimum design condition of $R_2 = 10$ μm. As can be seen from this figure, the coupling length is maximum at a cladding thickness $R_2 = 10$ μm. This can be correlated with Fig. 3, where the ISPM and the OSPM modes match very closely around 10 μm when the outer medium index, R_4 is 1.449. It can also be noticed from Fig. 4 that the maximum power transfer occurs without *E. coli* when the device length is around 1600 μm. However, at nearly the coupling length of around 1300 μm, maximum power transfers happen when there is a presence of *E. coli*. Hence, by carefully selecting the length of the fibre and monitoring power transfer, the presence of *E. coli* may be identified.

4.2 *Nanowires*

Optical fibres are relatively large compared to the wavelength and often show well confined optical modes. To access the evanescent field, a part of the cladding needs to be removed, as shown in the

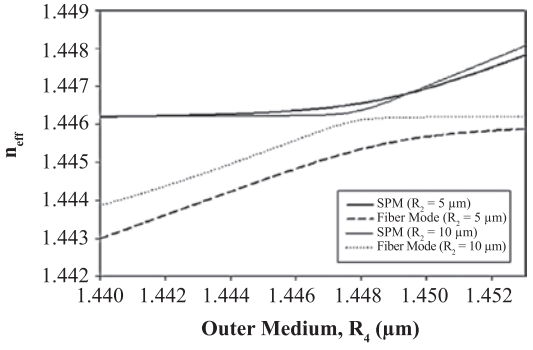

Figure 2: Effective index variation with the refractive index of the outer medium, R_4 for the inner and outer SPMs at the gold/cladding.

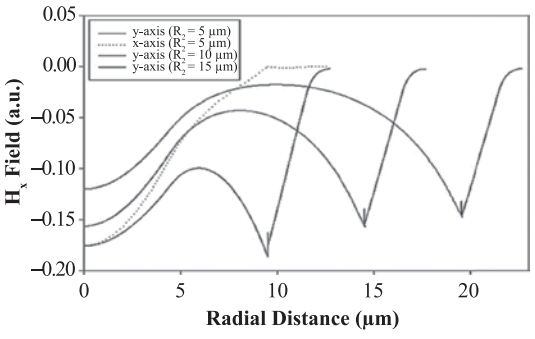

Figure 3: H_x field profile along the *y*-axis and *x*-axis for the outer SPM.

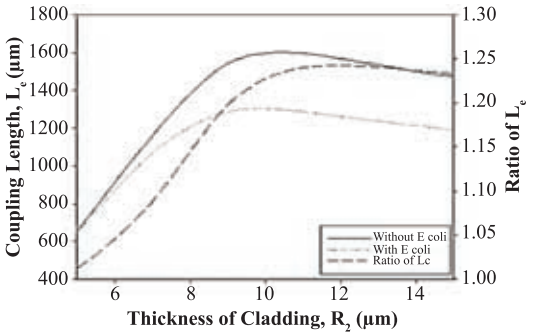

Figure 4: Coupling length as a function of the cladding thickness with and without *E. coli* for an outer medium index, R_4 of 1.449.

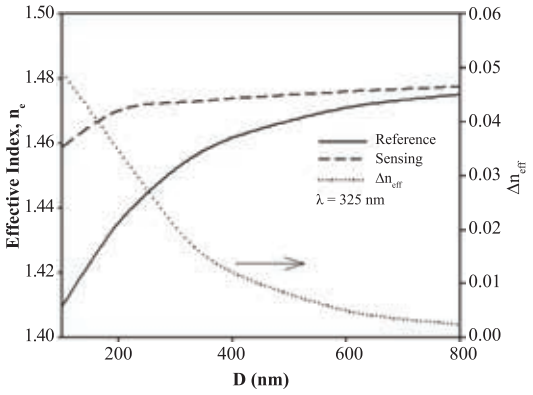

Figure 5: Effective index (n_e) and effective index difference (Δn_{eff}) between the reference and sensing arms as a function of the fibre diameter (D).

earlier example. However, when the waveguide is of sub-wavelength dimension as a nanowire, the mode extends appreciably at the boundary of the core, and this can be exploited to design more advanced optical sensors, as discussed below. With the improvement in manufacturing technology, sub-wavelength dimension nanowires are becoming increasingly viable optical sensors. As the core dimensions are often very small, it allows the access to higher field intensity at the waveguide surface for higher sensitivity of optical sensors.

To illustrate this, the variation of the effective reactive index of H_x[11] in the reference and the sensing arms with the silica nanowire diameter, D, has been examined, and the results are presented in Fig. 5. Here, the effective index of the reference arm and the effective index difference between the two arms is plotted against the core diameter, over a range of 100 nm to 800 nm. As can be seen from the aforementioned characteristics, as D decreases, the effective index also reduces and the rate of reduction slowly increases. The effective index difference between the reference and the sensing arm is presented in Fig. 5; however, this increases with the reduction of the core diameter. However, for a core diameter, D, of 100 nm, this exhibits a peak value, and as the core diameter increases further as this value reduces. This shows that a very small, 30 μm section of nanowire can provide 180° phase shift, useful for sensing applications.

4.3 *ZnO nanowires*

ZnO is a direct and wide band gap semiconductor material in the near UV range and it has a large excitonic process and large peizo-electric effect.[10] The new technologies such as controlling the conductivity of p- and n-type ZnO have also given the opportunity to promote the ZnO as the core material for photonic and opto-electronic devices, and also used as the solid state sensors for detecting the oxidizing and reducing gases.[11] In this part, the optical modal properties of the gold nanowire embedded in a ZnO cladding has been studied. This waveguide structure combines the advantages arising from the metal oxide and that of the surface plasmon.[12] The waveguide with a gold nanowire surrounded by a ZnO cladding has been analyzed using a full-vectorial FEM.

To expand this analysis, a gold nanowire surrounded by a Zinc Oxide cladding has been considered, as shown in Fig. 6. The nanowire has a radius, *r*, and the axis of the waveguide is assumed to lie in the Z direction. Exploiting the available symmetry, a quarter of the waveguide has been considered for the FEM analysis. The dispersion of the complex refractive index of gold has been obtained by an analytical formula given from Etchegoin *et al.*,[13] which considers the Drude's model with a high frequency limit dielectric constant and the inter-band transitions that occur in the violet and near

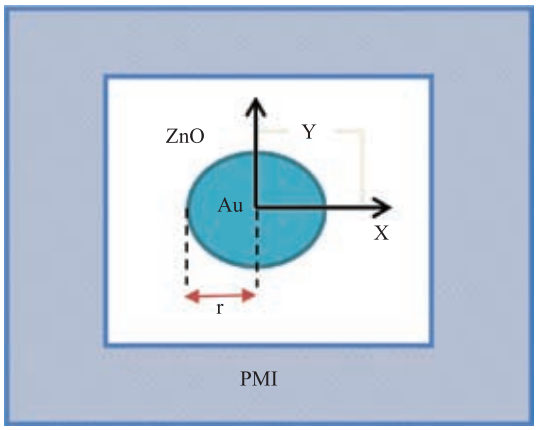

Figure 6: ZnO clad gold nanowire.

UV wavelengths. To include the effect due to finite cross section of the wire on the mean free path of the free electron in the gold nanowire, size dependent damping frequency has been included in the Drude's model.[14] Figure 7 shows the variation of the complex refractive index of a bulk gold with respect to the operating wavelength. The refractive index of the cladding, ZnO has been obtained from a formulation given by Holden[15] with the fitting parameters given by Jelllison.[16] The refractive index of undoped ZnO varies from between 2.2 and 2.0 for the range of wavelength that lies between 0.4 μm and 1.0 μm, while imaginary part of refractive index is nearly zero.

Figure 8 shows the dominant H_x field profile for the fundamental plasmonic H^x_{11} mode for a nanowire radius $r = 50$ nm at $\lambda = 0.70$ μm. It can be observed that the field decays exponentially in the ZnO cladding, however, within the metal it decays with damped oscillations. This can be explained as follows: The effective propagation constant determines the field profiles of the transverse and longitudinal electric field inside the gold nanowire, which in turn is determined by the difference between the effective dielectric constant of the mode and the complex dielectric constant of the gold. This results in either a sinusoidal or exponential field profile for the transverse and longitudinal electric (and magnetic) fields. The combination of transverse and longitudinal electric fields results in a damped oscillation superimposed on a decay profile for the H_x field inside the metal.

Figure 9 shows the variation of the attenuation with the operating wavelength for core radii r = 50 and 75 nm. As discussed earlier, as the confinement factor reaches a peak value around 0.50 μm, both loss curves also show a plasmonic resonance peaks around this wavelength. It can be observed that the loss value is higher for larger gold wire. It can also be noted that the variation of loss with respect to higher wavelengths shows

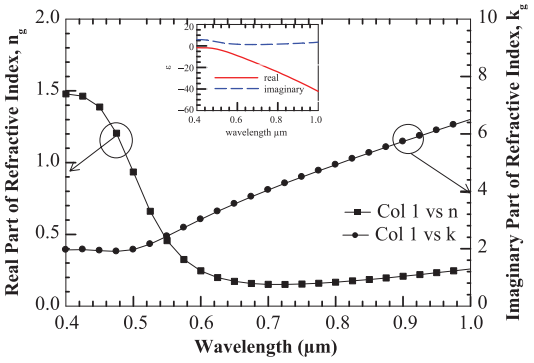

Figure 7: Complex refractive index of the gold nanowire (radius 50 nm).

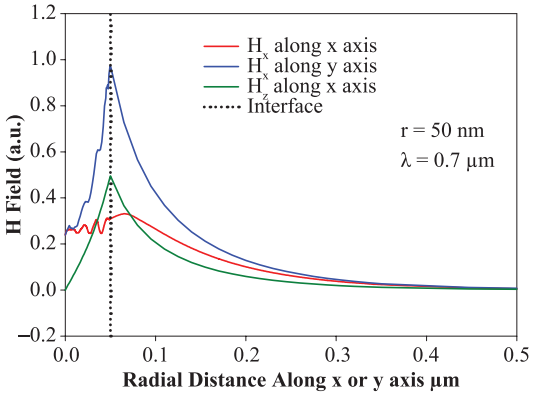

Figure 8: The H_x field profile of the SP mode for r = 50 nm.

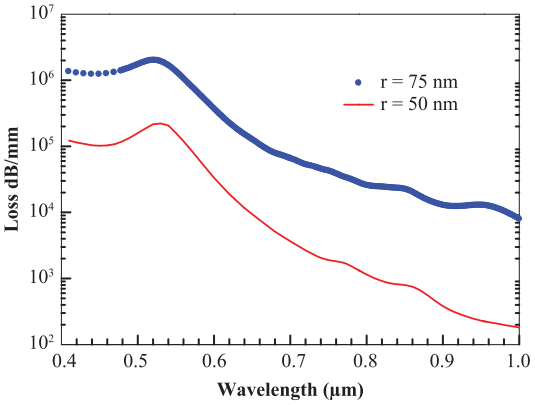

Figure 9: The variation of the loss with respect to the wavelength for two different radii r = 75 and 50 nm.

several smaller and smoother peaks. In Fig. 8, it has been shown that the H_x field profile inside the metal decays with damped oscillation. The resultant phase of these oscillations inside the H_x field profile varies with the wavelength, which results in the small oscillatory behaviour of the attenuation at the higher wavelengths. These oscillatory behaviours are also seen in the confinement factor, but they are only faintly visible in Fig. 9.

4.4 *Photonic crystal fibres*

Photonic crystal fiber (PCF) is a microstructured optical waveguide with low index air-holes running parallel to and along the length of the optical fibre,[17] which allows easy access to the evanescent fields. Recently polymer based PCF has also been demonstrated to guide terahertz waves (THz).[18,19] Modal properties of a metal-coated defect-core PCF with an air-hole at the center have been reported by using a full-vectorial finite element method (FEM).[1] Recently, PCF designs supporting a surface plasmon mode (SPM) using the

metal-coatings in the cladding region have been reported, designed for their applications in the optical frequencies.[20] A metal may be introduced in the central air-hole of a defect-core PCF in order to influence the modal properties significantly in the THz domain, studying their guidance properties for a range of potential applications, including evanescent sensing.[21] The structure suggested is one that is feasible as a design for fabrication with available technologies involving a) the deposition of metal-coatings on the microstructured fibres,[22] b) fabrication technology using Teflon to create the PCF,[23] c) techniques for copper coating on Teflon using Chemical Vapor Deposition[11] and d) metal-coated hollow waveguide technology.[24] Through tailoring the design of a PCF, it is possible to allow the coupling (which is tunable by varying the size of air-holes) between the SPMs at the metal-coated interface and the fundamental mode of a defect-core PCF (DCPCF). A H-field based rigorous full-vectorial FEM has been used to analyze a metal coated defect-core PCF (MCD-CPCF) operating at 1.0 THz.

The PCF design discussed here represents a holey microstructured fibre created from Teflon with a central air-hole defect. Figure 10 represents the cross-section of such a PCF with a metal-coated central air-hole. The complex refractive index of Teflon is considered to be $1.445 + j\,0.00119$ at 1.0 THz. The material cross section is accurately represented where all the air-holes are arranged in the triangular lattice, with the pitch length, Λ, being the distance between the air-holes and d the diameter of all the air-holes (except the central one). The radius of the central air-hole is R_A. Here the central air-hole has a metal coating of thickness τ. In the illustration, the background material shaded in the gray color represents the Teflon. A cladding region with three air-hole rings being considered in this rigorous evaluation of the PCF design.

Initially, the modal properties of a defect-core PCF without a metal coating ($\tau = 0$) was studied. The H_x fields of the fundamental quasi-TM (H^x_{11}) mode of this PCF at 1 THz (with $\tau = 0$, $d/\Lambda = 0.5$, $\Lambda = 2.0$ mm) for three different radii, $R_A = 0$, 0.05 and 0.01 mm are shown in Fig. 11. The field profile shown by a solid line is nearly Gaussian shaped when R_A is zero (without a defect-central air-hole). However, as R_A increases, the field deviates rapidly from the Gaussian profile with a dip in the centre of the core, showing a profound effect for even a smaller R_A. It can be seen from Fig. 11 that when $R_A = 0.05$ mm the field dips to 30% of the peak value (shown by a chained line) and when $R_A = 0.10$ mm (shown by dotted line) the field is

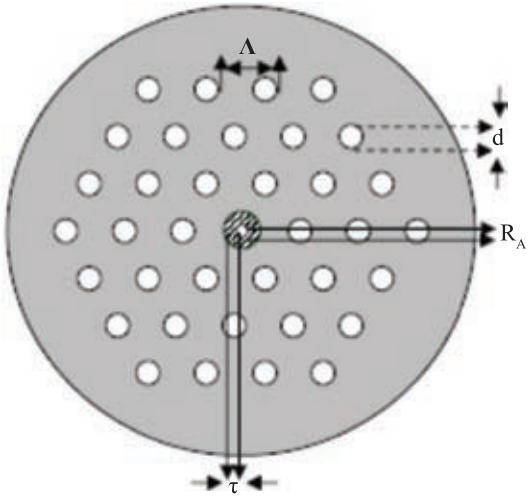

Figure 10: Cross section of a metal-coated defect-core PCF.

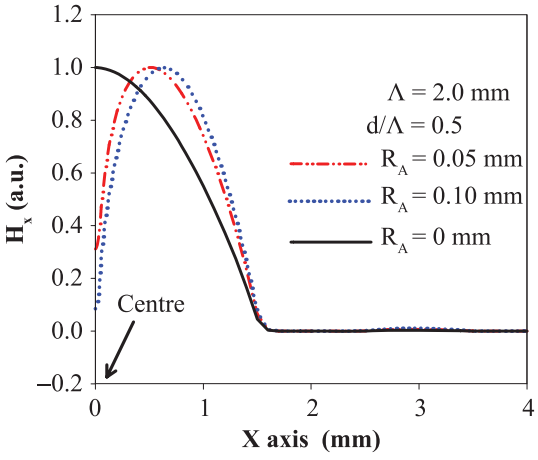

Figure 11: H^x_{11} mode for different defect hole radii $R_A = 0.0$, 0.5, 0.1 mm.

reduced to only 8% of the maximum value; when $R_A = 0.2$ mm (not shown here), the power confinement factor in the central air-hole Γ_A is only 0.0003, while with the air-holes in the cladding region, $\Gamma_{clad} \approx 0.0004$ and most of the remaining power is in the Teflon. Here, the Poynting vector was calculated from the H-field and this energy flux density may be integrated to obtain the power confinement factor in a particular region. The spot-size area for this case is around 7.0 mm^2 and the spot-size may be calculated by integrating the area with a field intensity higher than 1/eth of its highest value.

Figure 12 shows variations of effective index and the confinement factor with the R_A for $\Lambda = 1.0$ and 2.0 mm. The effective index is lower for a smaller pitch, $\Lambda = 1.0$ mm, as the mode is more

exposed to the cladding air-holes, compared to that of the larger pitch value. The effective indices also decrease with R_A as the equivalent index of the core reduces due to the enlarged central air-hole. It can also be observed that the rate of change is more profound for the smaller pitch length, as the mode is less confined for the smaller waveguide dimension. The confinement factor, Γ_A, initially increases with the R_A, and reaches a maximum value. With a further increase of R_A, the confinement factor Γ_A decreases, accompanied by an associated increase in the Γ_{clad}. As result, the modal loss starts to increase until the mode reaches a cut-off value, at around $R_A \leq d/2$. When $R_A = d/2$, the central defect air-hole is identical to the other air-holes; the structure becomes fully periodic without defects, and such a uniform medium without any defect cannot support a mode. It can also be observed that the value of Γ_A is large for the smaller pitch values, as the tightly packed air-holes lead to higher power confinement in the air-holes.

Subsequently plasmonic modes in such as metal-clad defect core PCF have been studied. The dielectric core of the PCF can support a nearly pure dielectric mode, as shown in Fig. 13a. However, a small plasmonic peak can be visible along the metal interface as shown by a dashed line. On the other hand, this waveguide also supports a nearly pure plasmonic mode, with high field intensity at the metal interfaces, as shown in Fig. 13b. By an appropriate design approach, these modes can be brought closer to phase matching. In that case, the presence of a small sensing medium can yield a drastic change in the modal properties, and this can be exploited to design very efficient sensors in the THz frequencies, as shown here.

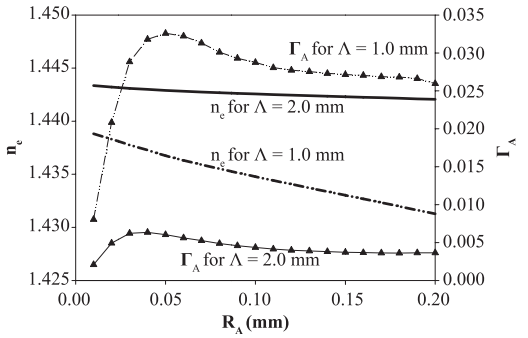

Figure 12: Variation of the confinement factor and effective index of the H^x_{11} mode with the central air-hole radius R_A.

4.5 *Slot waveguide structure*

Recently, the slot waveguide has emerged as a novel design where high field can be accessed in hollow or low-index region. In this case, the traditional Snell's law is no longer useful to explain the waveguiding in a low index region. The boundary condition at the dielectric interface demand that normal component of the H-field should be continuous. On the other hand, it also demands that the normal component of the D-vector should be continuous, which makes normal component of E vector non-continuous. This rather increases the E_n field to be higher in the low index region. This fundamental concept has been exploited in optical slot waveguide where two narrow waveguides, both operating below their modal cut-off regions are brought close together to generate a high electric field in the low-index region of the waveguide.

Such a novel slot waveguide has been investigated for the biosensing applications. The slot waveguide is formed by two Si wires close to each other having nanometer dimensions as shown in Fig. 14. The refractive index (RI) of silicon, silicon oxide and water are taken as 3.476, 1.444 and 1.31 respectively, at the operating wavelength of 1550 nm. In this design, the sensing structure is first coated with a linker layer (silanes) whose

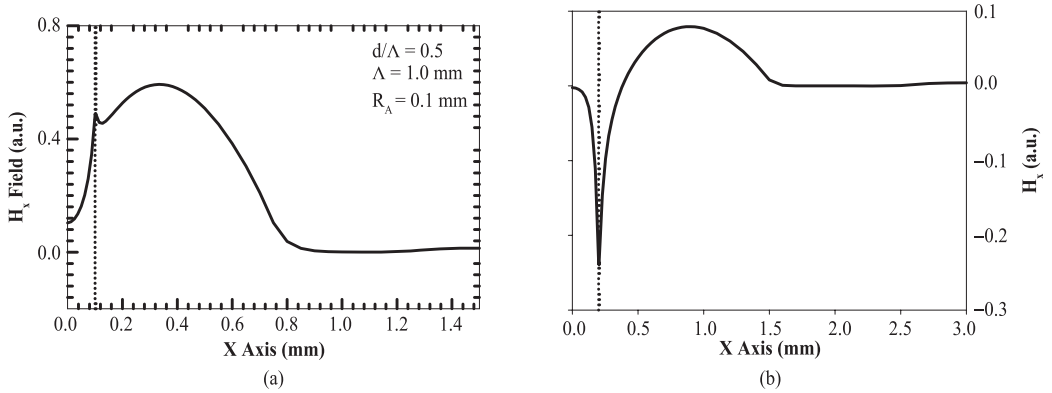

Figure 13: H_x field profile of (a) a dielectric mode and (b) a plasmonic mode in a MCDCPCF.

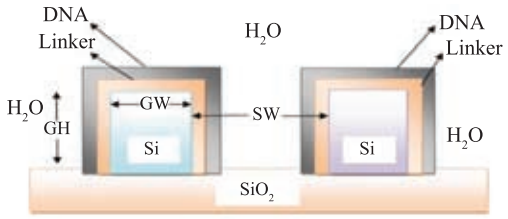

Figure 14: Slot waveguide biosensor.

refractive index is taken as 1.42 having a thickness of t = 1 nm. The actual sensing consists of detection of the complementary DNA sequence. The refractive index of ssDNA and dsDNA are taken as 1.456 and 1.53 respectively. The thickness of the DNA probe layer is taken as n = 8 nm, and remains unchanged when binding of complementary DNA strands (targets) to DNA probes happens, i.e. only the refractive index changes from 1.456 (ssDNA) to 1.53 (dsDNA). A waveguide height, GH = 320 nm, and high index region width, GW = 180 nm, slot width, SW = 100 nm, linker layer thickness of t = 1 nm, and DNA probe thickness of n = 8 nm, are considered for the initial simulation study. In similar structures, by optimising design approaches, nearly 40–50% power can be confined in the slot, but as the slot width is very small, ~100 nm wide, it produces a very high power density, or intense electric field which can be exploited. The effective index change was produced either by a change of cover medium refractive index (homogeneous sensing) or by a change of thickness of DNA layer, which is immobilized on waveguide surface (surface sensing). The measurement sensitivity depends on optical field distribution in the sensing medium, so one of the most important design task is the waveguide optimization in order to maximize its sensitivity. The adlayer thickness and change of cover medium refractive index affects the effective index of propagating optical mode. The thickness of the DNA probe layer is taken as 8 nm and remains unchanged when binding of complementary DNA strands (targets) to DNA probes happens and the refractive index of ssDNA and dsDNA are taken as 1.456 and 1.53 respectively. The waveguide sensitivity can be written as

$$S = \Delta n_{eff}/RI \quad (1)$$

where RI is the DNA layer refractive index and Δn_{eff} is the effective index difference when ssDNA and dsDNA are present. The effective index difference is achieved by simulating first by adding ssDNA layer on top of linker layer and then replacing the ssDNA by a dsDNA layer.

A waveguide height, GH = 320 nm is fixed, and SW = 60, 100 and 140 nm is varied. The sensing layers are linker layer (thickness t = 1 nm and RI = 1.42), ssDNA (thickness n = 8 nm and RI = 1.456), and water respectively. The ssDNA layer is replaced with the dsDNAlayer (thickness n = 8 nm and RI = 1.53) to achieve the difference between the two. Figure 15 shows larger effective index variation, and waveguide sensitivity is achieved at a guide width = 220 nm when the slot width is 60 nm, 100 nm and 140 nm respectively. The greater the change in Δn_{eff}, the more sensitive the biosensor will be. Therefore, when the guide width is between 200 nm and 220 nm maximum index difference is achieved. Although a smaller slot width shows a more sensitive design, while considering the fabrication techniques available today, a 100 nm slot-width is seen as a suitable design.

Figure 16 shows the change in effective index, and the waveguide sensitivity decreases with the increase in the slot width due to presence of DNA layers. A waveguide height, GH = 320 nm was fixed and GW was varied to equal 140, 180 and 220 nm in turn. The sensing layers are linker layers (thickness t = 1 nm and RI = 1.42), ssDNA (thickness n = 8 nm and RI = 1.456), and water respectively. The ssDNA layer has been replaced with

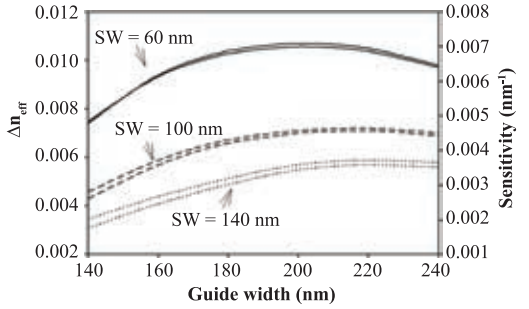

Figure 15: Variation of effective index difference, Δn_{eff} and waveguide sensitivity with guide width.

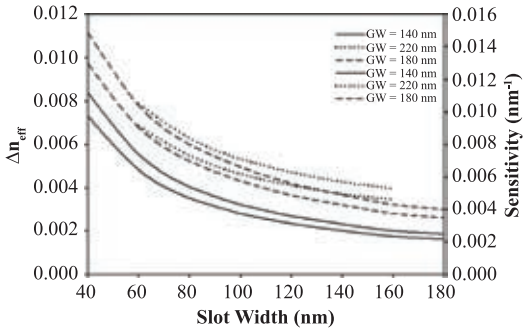

Figure 16: Variation of effective index difference, Δn_{eff} and waveguide sensitivity with slot width.

the dsDNA (thickness n = 8 nm and RI = 1.53) to achieve the difference between the two. A large effective index variation is achieved when the slot width is less than 100 in all cases. Although a smaller slot width shows a more sensitive design, considering the fabrication techniques available today, a 100 nm slot-width would be a more realistic design.

4.6 *Horizontal slots*

Although a horizontal slot may be easier to fabricate, and often have smoother interface, it will have a lower optical loss. However, the mode this structure would support would be the quasi-TM mode, as the discontinuity to E_y (which is normal to the dielectric interfaces here) is exploited here to have high power in the low-index region. The cross section of the horizontal slot waveguide structure on SOI substrate, where the low-index layer (slot) is sandwiched by two high-index poly-silicon layers, is presented in Fig. 17. The above structure is proposed to be used for bio sensing application, such as DNA hybridization. The sensor was designed to detect the change of effective index with the variation of the refractive index of the sensing material.

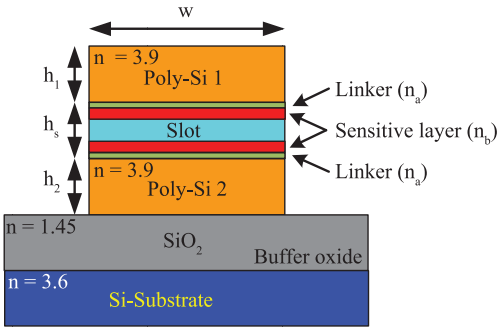

Figure 17: Cross section of the horizontal slot waveguide for sensing applications.

In this case, the sensing materials were assumed to be bonded with the thin linker layer inside the slot region. The linker, thus, was acting as glue in order to form the physical or chemical bonding with the sensing materials.

The change of the effective index of the horizontal slot waveguide may be investigated when single stranded DNA (ssDNA) becomes double stranded DNA (dsDNA), to detect the DNA hybridization, where the refractive indices of ssDNA and dsDNA are considered to be 1.456 and 1.53, respectively, at an operating wavelength of 1550 nm. The thickness ssDNA and dsDNA layers were taken to be fixed at 8 nm for the initial study. The refractive index of the poly-silicon core layers was considered to be 3.9 and water has been used as the material for the slot and cladding regions with a refractive index of 1.33. The refractive index (n_a) and the thickness of the linker layer, assumed to be silanes, are taken to be 1.42 and 1 nm, respectively. The key parameters optimized in the present work are the width (w), the poly-silicon core height (h_1 and h_2), and the slot height (h_s) of the structure.

In the modal solution of the FEM approach, half symmetry has been considered for the horizontal slot waveguide. The quasi-TM mode, where the dominant electric field is normal to the interface, is considered because it has a higher confinement in the slot region compared to the TE mode. For the quasi-TM mode, H_x field is the dominant component in the **H**-field. The contour of fundamental H_x field mode of the waveguide for a width (w) of 0.70 µm, poly-silicon core height of 0.16 µm and a slot height of 0.10 µm is presented shown in Fig. 18. The H_x field has a maximum intensity in both poly-silicon core layers. However, the maximum intensity is not in the centre of the core region, but is near to the interface between core region and the slot area as can be seen in the inset of Fig. 18(a).

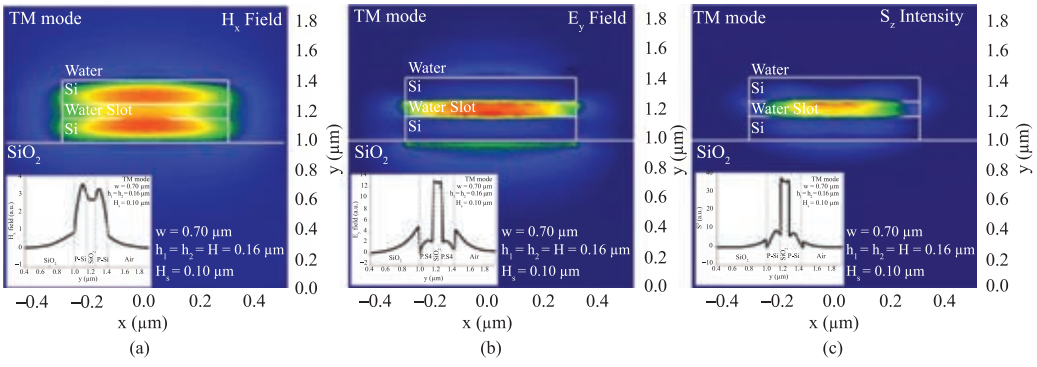

Figure 18: (a) H_x field, (b) E_y-field and (c) Energy flux density of the TM mode for the slot waveguide for w = 0.7 µm, $h_1 = h_2 = H = 0.16$ µm and $H_s = 0.10$ µm.

The fundamental E_y field has also been derived from the **H**-field solution and demonstrated in Fig. 18(b). The E_y field shows the discontinuity at the interface of core and slot regions providing the strong field in the slot area. The energy flux density so called Poynting vector (S^z) calculated from the **E** and **H** fields, is also presented in Fig. 18(c). It is clearly seen that the energy is more confined in the slot area, thus the light was guided in the low-index region for the slot waveguide.

The effect of the variation of the poly-silicon core height, *H*, which is considered to be symmetric ($h_1 = h_2 = H$), has been examined, where the width, w, and the slot height, h_s, are assumed to be fixed at 0.7 μm 0.10 μm, respectively. The power confinement and the power intensity in the sensing layer (DNA probe) with the variation of the core height are presented in Fig. 19.

The power confinement in Fig. 19 is the sum of the power confinement in upper and lower DNA probe layers having a thickness of 8 nm each. The power density is the average power density for both DNA probe layers. The power confinement and power density exhibit similar trend when the core height is varied. At the smaller core height, both power confinement and power density in the sensing layers are initially low because it is closed to the cut off. Therefore, the optical power losses occur due to an evanescent wave spreading into the cladding medium and the buffer oxide layer. Then the power increases with the core height, due to enlargement of guided area, until reaching a maximum confinement at a height, H, of 0.15 μm. However, if the core height is too large, the light will mainly be guided only inside the poly-silicon core region. Consequently, the power confinement and power density are decreased as the core height increases further. It is also observed that ssDNA ($n_b = 1.456$) has higher power in the sensing medium compared to the dsDNA ($n_b = 1.530$). This is due to higher refractive index contrast in ssDNA, which leads to the larger discontinuity in electric field.

One of the most important parameters in biosensing applications is the change of effective index, used to calculate for the sensitivity of the device. The change of effective index with respect to the core height is shown in Fig. 20, where the effective index of each sensing material also may be included.

The change of effective index increases when the core height is increased until it reaches a maximum point at height of 0.17 μm. At a height greater than 0.17 μm, the structure becomes too large, and the light more confined to the core than in the slot. This leads to a reduction of the change of effective index as well as the sensitivity of the waveguide. By considering individually, the ssDNA has a lower effective index compared to the dsDNA due to the smaller refractive index, which is 1.456. However, the effective index increases when the poly-silicon core height is increased for both ssDNA and dsDNA, because of the stronger coupling.

From the results presented earlier in Fig. 19, the optimum core height for obtaining maximum power was found to be about 0.16 μm, and therefore, the above dimension was set at 0.16 μm and the slot height at 0.10 μm in the study of the effect of the structure width. The thickness of linker layer (silanes) and the sensing medium (DNA) remained the same at 1 nm and 8 nm, respectively. The power confinement and the power density with the variation of the width of the waveguide are presented in Fig. 21.

At smaller width, the power confinement in the slot region is less due to the smaller size of the structure, where the mode approaches cut-off. Therefore, only some light is guided in the guiding region, and the rest is spread

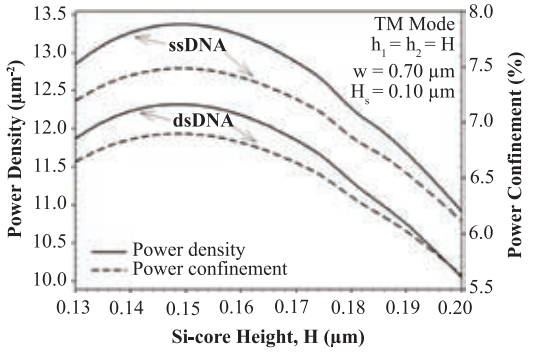

Figure 19: Variation of power density and power confinement in the sensing layer (DNA probe) with the core height, H.

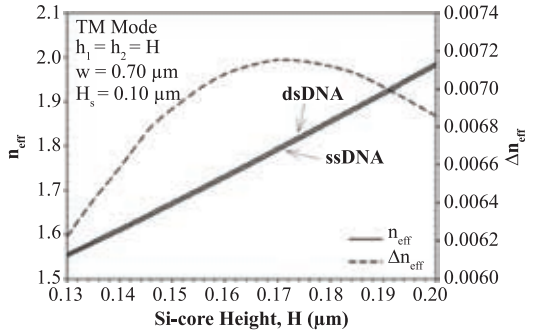

Figure 20: Variation of the effective index difference and the effective index in each sensing material with the core height.

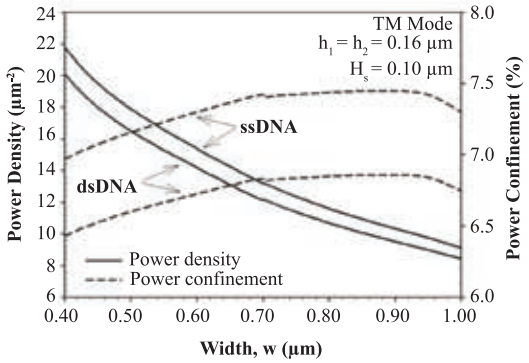

Figure 21: Variation of the power density and power confinement in the sensing layer (DNA probe) with the width.

into the cladding region. When the width is increased, the power confinement is also slightly increased. In the case of the ssDNA (n_b = 1.456), the power confinement is higher than that of the dsDNA (n_b = 1.530) due to the higher refractive index contrast. On the other hand, the power density is inverse proportional to the width. At a smaller values of width, the power density is high because the guiding area is less. As the width increase, the power per area is reduced due to the larger guiding area. However, a higher power density is observed in the ssDNA than in the dsDNA due to higher power confinement.

5 Conclusions

The basic principle of optical sensing and the numerical methods needed for simulations in a range of sensor designs are discussed. Numerically simulated results for some well-established sensors, such as simple polished metal clad single mode fibres, and the fast emerging silica nanowires are presented. Besides that, a metal clad ZnO based gas sensing concept has also been presented. The design concept for emerging THz technology and its application in sensing using metal-clad defect core photonic crystal fibres have also been shown/handled. Finally, exploiting advances in the CMOS manufacturing technology, the design optimization of both vertical and horizontal slots for bio-sensing applications have been demonstrated.

It should be noted that for optical guided wave structures with strong index confinement, the modal fields are fully vectorial in nature. The exotic waveguides, such as those seen for microstructured photonic crystal fibre, has an intricate air-hole arrangements in the core. Similarly the refractive index of the metal layers, or doped ZnO are complex in nature. So, for the design optimization full vectorial and numerically efficient approaches should be used.

Received 23 July 2014.

References

1. B.M.A. Rahman and J.B. Davies, "Finite-element solution of integrated optical waveguides," *IEEE/OSA J. Lightwave Technol.* 2, 682–688, 1984.
2. M.D. Feit and J.A. Fleck Jr., "Light propagation in graded-index optical fibers," *Appl. Opt.* 26, 3990–3998, Dec 1978.
3. S.A.A. Obayya, B.M.A. Rahman and H. El-Mikathi, "New fullvectorial numerically efficient propagation algorithm based on the finite element method," *IEEE/OSA J. Lightwave Technol.* 409–415, March 2000.
4. M. Heiblum and J.H. Harris, "Analysis of curved optical waveguides by conformal transformation," *IEEE J. Quantum Electron.* **11**, 75–83, 1975.
5. B.M.A. Rahman and J.B. Davies: "Analyses of Optical Waveguide Discontinuities," *IEEE/OSA J. Lightwave Technology* 52–57, Jan. 88.
6. T. Makino, Transfer matrix method with applications to distributed feedback optical devices, 271–319, in "Methods for Modelling and Simulation of Guided-wave Optoelectronic Devices: Part I: Mode and Coupling," Ed. W P Huang, *PIER Series* 10, 1995.
7. A. Taflove, and S.C. Hagness, "Computational Electrodynamics: The finite difference time-domain method", Artech House, 2005.
8. Y. Liu, B.M.A. Rahman and K.T.V. Grattan, "Thermal stress induced birefringence in bow-tie optical fibers using the finite element method", *Applied Optics* 33, 5611–5616, August 1994.
9. S. Sriratanavaree, B.M.A. Rahman, "Rigorous characterization of acoustic-optical interactions in silicon slot waveguides by full-vectorial finite element method," *OSA Optics Express* 9528–9537, 2014.
10. A. Janotti and C.G. Van de Walle, "Fundamentals of zinc oxide as a semiconductor," *Rep. Prog. Phys.* 72, 126501, 2009.
11. D.D. Lee and D.S. Lee, "Environmental gas sensors," *IEEE Sensors* 1 214–224, 2001.
12. S.A. Maier, "Plasmonic Fundametals and Applications," Springer, 2007.
13. P.G. Etchegoin, E.C. Le Ru and M. Meyer, "An analytic model for the optical properties of gold," *The Journal of Chemical Physics* 125, 164705, 2006.
14. J.A. Gordon and R.W. Ziolkowski, "The design and stimulated performance of a coated nano-particle laser," *Optics Express* 15, 2622–2653, 2007.
15. T. Holden, P. Ram, F.H. Pollak, J.L. Freeouf, B.X. Yang, and M.C. Tamargo, "Spectral ellipsometry investigation of Zn0.53Cd0.47Se lattice matched to InP," *Phys. Rev.* B 56 4037, 1997.

16. G.E. Jellison Jr and L.A. Boatner, "Optical functions of uniaxial ZnO determined by generalized ellipsometry," *Physical Review* B 58 3586–3589, 1998.
17. P. St. J. Russell, "Photonic-Crystal Fibers," *J. Lightwave Technol.* 24, 4729–4747, 2006.
18. H. Han, H. Park, M. Cho and J. Kim, 'Terahertz pulse propagation in a plastic photonic crystal fiber,' *Appl. Phys. Lett.* 80, 2634–2636, 2002.
19. M. Goto, A. Quema, H. Takahahi, S. Ono, and N. Sarukura, "Teflon photonic crystal fiber as terahertz waveguide," *Jpn. J. Appl. Phys* Part 2 43, L317–L319, 2004.
20. J. Hou, D. Bird, A. George, S. Maier, B.T. Kuhlmey and J.C. Knight, "Metallic mode confinement in microstructured fibres," *OSA Opt. Express* 16, 5983–5990, 2008.
21. A. Hassani and M. Skorobogatiy, "Design criteria for microstructured-optical fiber based surface-plasmon-resonance sensors,"*OSA JOpt. Soc. Am.* B 24, 1423–1429, 2007.
22. P.J.A. Sazio, A. Amezcua-Correa, C.E. Finlayson, J.R. Hayes, T.J. Scheidemantel, N.F. Baril, B.R. Jackson, D.J. Won, F. Zhang, E.R. Margine, V. Gopalan, V.H. Crespi, and J.V. Badding, "Microstructured optical fibers as high pressure microfluidic reactors," *Science* 311, 1583–1586, 2006.
23. T.Y. Chen, C. Combellas, P. Doppelt, F. Kanoufi, A. Thiébault, "Selective Metallization of Mg/NH3-Treated Teflon by Copper CVD," *Chemical Vapor Deposition* 5, 185–190, 1999.
24. J.A. Harrington, R. George, P. Pederson and E. Mueller, "Hollow polycarbonate waveguides with inner Cu coatings for delivery of terahertz radiation," *OSA Opt. Express* 12, 5263–5268, 2004.

Prof. B.M. Azizur Rahman received the B.Sc. Eng and M.Sc. Eng. degrees in Electrical Engineering with distinctions from Bangladesh University of Engineering and Technology (BUET), Dhaka, Bangladesh, in 1976 and 1979, respectively. He also received two gold medals for being the best undergraduate and graduate students of the university in 1976 and 1979, respectively. In 1979, he was awarded with a Commonwealth Scholarship to study for a PhD degree in the UK and subsequently in 1982 received his PhD degree in Electronics from University College London.

In 1988, he joined City University, London, as a lecturer, where he is now a Professor. At City University, he leads the research group on Photonics Modelling, specialised in the use of rigorous and full-vectorial numerical approaches to design, analyse and optimise a wide range of photonic devices, such as spot-size converters, high-speed optical modulators, compact bend designs, power splitters, polarisation splitters, polarisation rotators, polarization controllers, terahertz devices, etc. He has published more than 450 journal and conference papers, and his journal papers have been cited more than 2800 times with h-factor of 26.

Prof. Rahman is a Senior Member of IEEE (USA), and Fellow of the Optical Society of America, and of the SPIE.

Dr. N. Kejalakshmy received the Ph.D. degree in physics in the research of crystal growth and nonlinear optical properties of crystals from Indian Institute of Technology (IITM), Madras, India, in 2003. Since 2005 she has been working as a Research Fellow in City University London, U.K. Her research interest includes numerical modeling of waveguides and optical sensors in optical and Terahertz frequencies using finite element and beam propagation methods.

Charusluk Viphavakit was born in Bangkok, Thailand, on December 18, 1987. She received the Bachelor's degree in nano-electronic engineering from Chulalongkorn University, Bangkok, Thailand, in 2010 and the Master's degree in nanotechnology from Asian Institute of Technology (AIT), Pathumthani, Thailand, in 2012. She is currently pursuing the Ph.D. degree in electrical engineering at Frederick University, Nicosia, Cyprus.

In 2012, she received a scholarship from European Union's Erasmus Mundus program for her Ph.D. Her research interests include the design, development and characterization of integrated optics nanowires using finite-element method, the study of surface plasmon properties on nanowires including their sensing applications, and the fabrication of semiconductor and polymer sub-micron nanowire.

Ms. Viphavakit is a student member of the Optical Society of America and a student member of SPIE.

Prof. Christos Themistos received the B.Eng. and Ph.D. degrees in electrical engineering from the City University, London, U.K., in 1992 and 1998, respectively. His Ph.D. degree involved the development of a finite-element-method-based approach, in conjunction with the perturbation technique, for the analysis of loss and gain in optical waveguides.

His research interests involve the application of finite-element-based approaches for the characterization of photonic devices, such as multimode interference-based designs, optical modulators, and the analysis of surface plasmon modes in optical waveguides at optical and terahertz frequencies. Since 2000, he has been with the Photonic Devices Modelling group at the City University, and the Frederick Research Centre, Cyprus, and he has been involved in projects funded by the industry, the Research Promotion Foundation, Cyprus, and the Royal Society, U.K.

Prof. Muttukrishnan Rajarajan (Raj) is a Professor of Security Engineering and leads the Information and Cyber Security Research activities at City University London. He has expertise in the areas of mobile security, cloud security, network security and critical national infrastructure protection for well over 15 years. He acts as an advisor to the government of India Advanced computing research laboratories in the area of cyber security. He is a visiting fellow at the British Telecommunications security laboratories. He has been involved in several recent policy debates and scoping workshops in the area of cyber security, identity management and Cloud security. Raj has published more than 200 journal and conference papers and has recently published a book entitled *Mobile Security and Privacy.* He is also actively engaged in the UK National Crime Agency Cyber Security activities and leads on the UK government's Identity Assurance initiative. Raj is currently working with several government offices and the public sector partners to generalise the UK government's identity assurance scheme. He is also working with the intelligence services to link the social identity (i.e. Social media identity) with the physical identify of individuals. He serves on several editorial boards and international conferences programme committees. He has been the General Chair of *Securecomm* 2011 and Technical Programme Committee Chair of *Security of Information and Networks* 2014. He was the Guest Editor of a special issue on Springer Journal of Mobile Networks in Wireless Security and Privacy. He is also on the Editorial Board of Springer Journal of Wireless Networks. Raj recently led the security and trust work stream of a (11M European Union Framework 7 project OPTIMIS (Optimised Infrastructure Services). As part of this project his team built the first peer-to-peer overlay architecture for secure communication in an inter-cloud environment. In addition to this he and his team proposed a cloud broker architecture which is currently deployed in the BT's Cloud environment. Raj is a Senior Member of Institute of Electrical and Electronic Engineering (IEEE-USA) and is a member of the academic advisory board of the institute of information security professionals (IISP), UK.

Professor K.T.V. Grattan graduated in Physics from Queen's University Belfast with a BSc (First Class Honours) in 1974, followed by a PhD in Laser Physics in the use of laser-probe techniques for measurements on potential new dye laser systems.

In 1978 he became a Research Fellow at the Imperial College of Science and Technology, (sponsored by the Rutherford Laboratory) to work on advanced photolytic drivers for novel laser systems. In 1983 he joined City University as a "new blood" Lecturer in Physics, being appointed Professor of Measurement and Instrumentation and Head of the Department of Electrical, Electronic and Information Engineering in 1991. His research interests have expanded to include the use of fibre optic and optical systems in the measurement of a range of physical and chemical parameters. He obtained a DSc from City University in 1992 for his work in sensor systems and became Chairman of the Science, Education and Technology of the Institution of Electrical Engineers, the Applied Optics Division of the Institute of Physics and he was President of the Institute of Measurement and Control during the year 2000. He was awarded the Callendar Medal, the Honeywell Prize and the Hartley Medal of the Institute of Measurement and Control and was Dean of the School of Engineering & Mathematical Sciences and the School of Informatics at City University from 2008 to 2012. He was appointed Dean of the City Graduate School in 2012. He was elected to the Fellowship of the Royal Academy of Engineering in 2008.

He is the author of over seven hundred publications in major international journals and conferences and is the co-editor of a five volume topical series on Optical Fibre Sensor Technology.